Fast Track

Zachary Gagnon
Satyajyoti Senapati
Jason Gordon
Hsueh-Chia Chang

Department of Chemical and Biomolecular Engineering, Center for Microfluidics and Medical Diagnostics, University of Notre Dame, Notre Dame, IN, USA

Dielectrophoretic detection and quantification of hybridized DNA molecules on nano-genetic particles

DNA–DNA hybridization reactions on 100 nm oligonucleotide-functionalized silica nanoparticles are found to sensitively affect the amplitude and direction of the dielectrophoretic mobility of the particles at nanomolar target ssDNA concentrations. Such sensitivity permits visual detection of the hybridization event without fluorescent labeling and confocal microscopy by imaging the cross-over frequency (*cof*) of the particle suspension on a quadrupole electrode array. Strong correlation with effective particle radius and zeta-potential measurements suggests that the dielectrophoretic *cof* offers not just sensitive signatures for successful functionalization and hybridization but also those for three distinct DNA surface conformations that appear at different surface densities of hybridized DNA. A properly normalized *cof* calibration chart allows simplified quantification of the target ssDNA concentrations. These results provide a simple, rapid and portable genetic detection method compatible for use outside the laboratory.

1 Introduction

The DNA–DNA micro-array has become a widely used laboratory tool for genetic detection due to robustness, sensitivity and large sample throughput that such arrays offer. While often time consuming, typically on the order of hours to days, the standard micro-array technique is relatively simple to perform and allows for highly sensitive multi-target analysis. However, such techniques are typically analyzed *via* florescent microscopy, and therefore usually limited for use on the laboratory benchtop. The ability to quickly and accurately detect molecular events outside the laboratory is a necessary requirement in next generation genetic assays and portable point-of-care diagnostic devices. While there has been interest in developing this area, most detection schemes available are still dominated by varying forms of simplified electronic, electro-optical or fluorescence

detection schemes [1, 2]. Here, we present an alternative approach to in-field genetic testing, which does not require the use of florescent probes. Instead, we demonstrate a sensitive, simple, label-free and robust dielectrophoretic hybridization detection and analysis scheme based on carboxylated silica nanoparticles.

2 Theory

Dielectrophoresis (DEP) is a term used to describe the movement of polarizable particles induced by a non-uniform alternating current (AC) electric field and has been widely used in cellular and colloid manipulations [3–6]. The dielectrophoretic force on a particle of radius a, suspended in a medium permittivity ϵ_m in an AC field of magnitude E is $2\pi a^3 \epsilon_m \text{Re}[f_{cm}]\nabla|E|^2$, and results from induced AC particle dipoles developed by either conductive or dielectric polarization mechanisms as determined by the Clausius–Mossotti (CM) factor, $f_{cm} = (\epsilon_m^* - \epsilon_p^*)/(\epsilon_p^* - 2\epsilon_m^*)$. The complex permittivity ϵ^* is related to the real permittivity ϵ and conductivity σ *via* the AC field frequency ω for both the particle (p) and the medium (m). Each is described by $\epsilon^* = \epsilon + \sigma/(i\omega)$, with the permittivity, ϵ, dominating dipole formation at high frequencies, and conductivity, σ, at low frequencies. A positive real part to the CM factor indicates that the DEP force pushes a polarized particle towards a local electric field maximum, which is known as positive DEP, while a negative CM factor pushes the particle away from the field maximum and into

Correspondence: Professor Hsueh-Chia Chang, Department of Chemical and Biomolecular Engineering, Center for Microfluidics and Medical Diagnostics, University of Notre Dame, 182 Fitzpatrick Hall, Notre Dame, IN 46556, USA
E-mail: hchang@nd.edu
Fax: +1574-631-8366

Abbreviations: AC, alternating current; **CM,** Clausius–Mossotti; **cof,** cross-over frequency; **DEP,** dielectrophoresis; **EDC,** 1-ethyl-3-(3-dimethylaminopropyl) carbodiimide hydrochloride; **NHS,** sulfo-*N*-hydroxysuccinimide

regions of weak electric field, known as negative DEP. The frequency at which the CM factor equals zero is known as the cross-over frequency (*cof*) [2]. The different mobility directions on each of the two sides of the *cof* offer very sensitive means of separating and identifying bioparticles and colloids with different *cof*s, as most other analytical techniques for colloids and molecules exploit only the difference in the mobility amplitude. Recent studies of nanocolloid DEP demonstrate that σ_p and the *cof*s of sub-micron particles are sensitive to surface conductance/charge changes due to docking of molecules of comparable size [7, 8], suggesting that macroscopic nanoparticle suspension patterns near an electrode array can reflect molecular docking events. Nanocolloids are already used in many molecular assays [9] because of the sensitivity offered by their size-to-volume ratio (we shall demonstrate nM sensitivity in the current experiment) and their docking speed for mass-transfer-limiting docking reactions because of their number. If the nanoparticle suspensions also offer high sensitivity to the docking events, without labeling and fluorescent detection, a DEP/nanoparticle platform may fundamentally change DNA, protein and other molecular identification assays.

In this work, we demonstrate the ability to detect and characterize a hybridization reaction on the surface of a 100 nm oligo-functionalized silica particle without the use of florescent tags or confocal microscopy at 5–100 nM target DNA concentrations. We detect hybridization dielectrophoretically using particle-distinct *cof*s. Our analysis reveals that hybridized nanoparticles have *cof*s that are highly dependent upon the concentration and conformal structure of the hybridized ssDNA.

3 Materials and methods

To functionalize the genetic particles, a suspension of 2.5 wt% 100 nm carboxylated silica particles (microspheres–nanospheres) was diluted fourfold and suspended in a 2:1 molar buffer solution of 1-ethyl-3-(3-dimethylaminopropyl) carbodiimine hydrochloride (EDC) and sulfo-*N*-hydroxysuccinimide (NHS), respectively. Single stranded oligonucleotide fragments (Invitrogen) 27 bases in length were then added in concentrations of 0.01, 0.025, 0.05, 0.1, 1 and 2 μM to aliquots of the buffer solution for a total of six samples, and agitated for 4 h. The two buffers serve to stabilize the reaction. EDC reacts with the carboxyl group present on the particle surface forming an unstable reactive *o*-acyl ester intermediate, which when coupled with NHS forms a semistable NHS-ester intermediate that reacts with the amine group on the oligo backbone, resulting in an oligo-functionalized silica particle *via* an amide bond [10]. The particles were passivated in 1 M Tris-HCl overnight to remove any unreactive semi-stable intermediate to prevent non-specific chemical adsorption of ssDNA. The suspension of particles was then washed three times in 1 M sodium chloride/sodium citrate buffer (Sigma-Aldrich) and stored at 10°C until ready to undergo hybridization with ssDNA.

The ssDNA fragments (1000 bases) were synthesized by asymmetric PCR using the identical oligonucleotide primers that were used in the functionalization reaction on *Escherichia coli* strain PU-C17. Prior to hybridization, ssDNA fragments were diluted fivefold into 1 M sodium chloride/ sodium citrate buffer for a final ssDNA concentration of approximately 100 nM determined *via* absorbance measurements. The resulting ssDNA sample was then added to aliquots of functionalized genetic particles in concentrations of 5, 20, 50, 100 and 150 nM and incubated for 8 h at 50°C to ensure complete hybridization, resulting in 30 samples. A sample consisting of non-functionalized ''naked'' particles was also incubated with each ssDNA sample to serve as an experimental control. It should be noted that due to such a high surface-to-volume ratio, we have been able to successfully hybridize the nanoparticles with a 10 min incubation step; however, this will be properly addressed in a separate work. Each sample was then washed three times and suspended in 18.2 MΩ water prior to analysis.

DEP experiments under the optical microscope (Labsmith SVM340) were performed on a quadrupole electrode array. The electrodes were fabricated onto pre-cleaned 50×75 mm glass slides. Slides were patterned with the image reversal photoresist Shipley AZ-5214 to define the electrode patterns, after which 50 of titanium and 2500 of gold were evaporated onto the slides. This was followed by a resist dissolution and metal liftoff in acetone. The arrays were designed as four triangular posts with an inner square side length of 25 μm and an electrode width of 60 μm.

The fabricated array, as shown in Fig. 1, was attached to a function generator set to 10 Vpp (Agilent, model ♯ 33220A) *via* copper tape and wire leads, which yielded the center region of the four electrodes an absolute field minimum and the electrode edges an absolute field maximum.
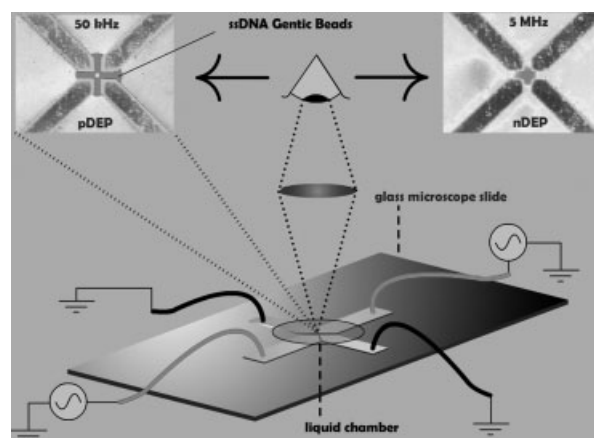

Figure 1. A schematic view of the experimental setup used in the DEP experiments under the microscope. The solution containing the genetic particle suspension is housed in the containment chamber and in contact with the quadrupole electrode array. The electric field is applied and the *cof* is measured by determining when the particles switch from positive DEP (top left image) to negative DEP (top right image).

A plastic coverslip was then placed over the array followed by injection of the hybridized particle suspension upon which the frequency was slowly increased from 50 kHz to 5 MHz in order to determine the *cof*. As shown in the figure, the suspension *cof* was taken when the genetic particles migrated from the electrode edges (image top left) to the electrode center (image top right). The particle size and zeta potential were measured (Brookhaven Instruments Zeta Pal 3100) as a function of both oligo and ssDNA concentration before and after hybridization.

4 Results and discussion

Four possible conformational structures can be expected of the hybridized ssDNA, which is much longer than the oligo. Non-specific interaction between individual hybridized nucleotides with the silica surface, due to electrostatic interaction between the charged DNA and heterogeneities on the silica surface, can produce a collapsed structure (Fig. 2A). Electrostatic monomer repulsion can result in a stretched conformation (Fig. 2B) where the nucleotides are essentially perpendicular to the colloid surface. Elastic contraction can produce an entropic DNA brush structure with a loose random-walk coil [11] and DNA coil condensation at the end of the hybridized DNA can produce a tight coil [12]. The elastic coil and the condensed coil may not be differentiable (Fig. 2C). However, one expects the condensed coil to be energetically favored at high DNA surface concentrations because electro-static monomer repulsion is reduced by the screening of the DNA charge in the condensed coiled conformation [13].

Initial experiments indicated that bare unfunctionalized colloids and the "naked" control sample both had a measured *cof*, effective diameter and zeta potential of 500 kHz, 102 nm, and -26.45 ± 0.6 mV, respectively. Upon functionalization, as shown in Fig. 3A, one can observe a steady increase in effective diameter with an increase in oligo concentration from 102 nm to that of an average value of approximately 118 nm at an oligo concentration beyond 0.1 µM. This measurement is approximately equal to the theoretical diameter of a 100 nm particle functionalized with a 27 base length oligonucleotide, assuming 1 base length is approximately 0.34 nm in length [5], suggesting successful oligo functionalization. Measured zeta potential for the

functionalized particle, as shown in Fig. 3A, first drops to -11.5 mV from the unfunctionalized value of -26.5 mV at oligo concentrations below 0.01 µM, and then increases to almost the bare particle value at 0.025 µM. Beyond this concentration, however, the zeta potential increases monotonically with respect to the oligo concentration and saturates at 0.1 µM, with the same trend as the effective particle size. The *cof* measurement, as shown in Fig. 3B, jumps by a factor of 4 with slight functionalization, followed by a sharp drop below 0.05 µM. Beyond this concentration, the *cof* increases with respect to the oligo concentration for all oligonucleotides, and saturates at the oligo concentration of 0.1 µM. The absolute minimum value in the zeta potential occurs near the same concentration as the minimum in the *cof*. We are currently unable to explain the sharp change of both bare and slightly functionalized particles, and their non-monotonic dependence on the oligo concentration. However, it is quite clear from all three measurements that surface oligo saturation occurs on the carboxylated silica at 0.1 µM and the corresponding *cof* is a factor of 4 higher than the unfunctionalized bare particles.

Hybridization analysis was performed on a suspension functionalized with an oligo concentration of 0.05 µM. The effective diameter as a function of ssDNA concentration is shown in Fig. 3C. It was interesting to observe a maximum effective diameter of 738 nm at an ssDNA concentration of 25 nM, followed by a steady decline to an asymptotic value of 630 nm. Measurements of the suspension zeta potential exhibited a similar trend, with a maximum absolute value of -17.5 mV at an ssDNA concentration of 20 nM. The measured suspension *cof*, shown in Fig. 3D, also show strong correlations to the effective particle size and the absolute zeta potential, with a clear maximum of 2.4 MHz at 20 nM DNA concentration. At this optimum target DNA concentration, the *cof* is more than 500 kHz higher than the value for unhybridized oligo-functionalized nanoparticles (compare Fig. 3B and D at 0.05 µM oligo concentrations). This differential in *cof* is more than 100 times the experimental resolution of our equipment, indicating that *cof* is indeed a very sensitive means of detecting hybridization. Moreover, due to the sensitivity of the *cof* to surface density of docked target DNAs, Fig. 3D represents a sensitive calibration curve for target DNA concentrations above 20 nM.

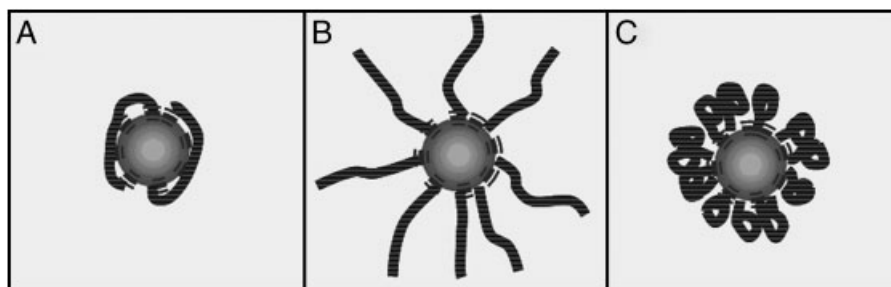Identical analyses were repeated with DNA and oligo concentrations ranging from 0.1 to 2 µM and 5–150 nM,

Figure 2. (A–C) Different possible conformations of DNA molecules hybridized to the surface of silica nanoparticles.
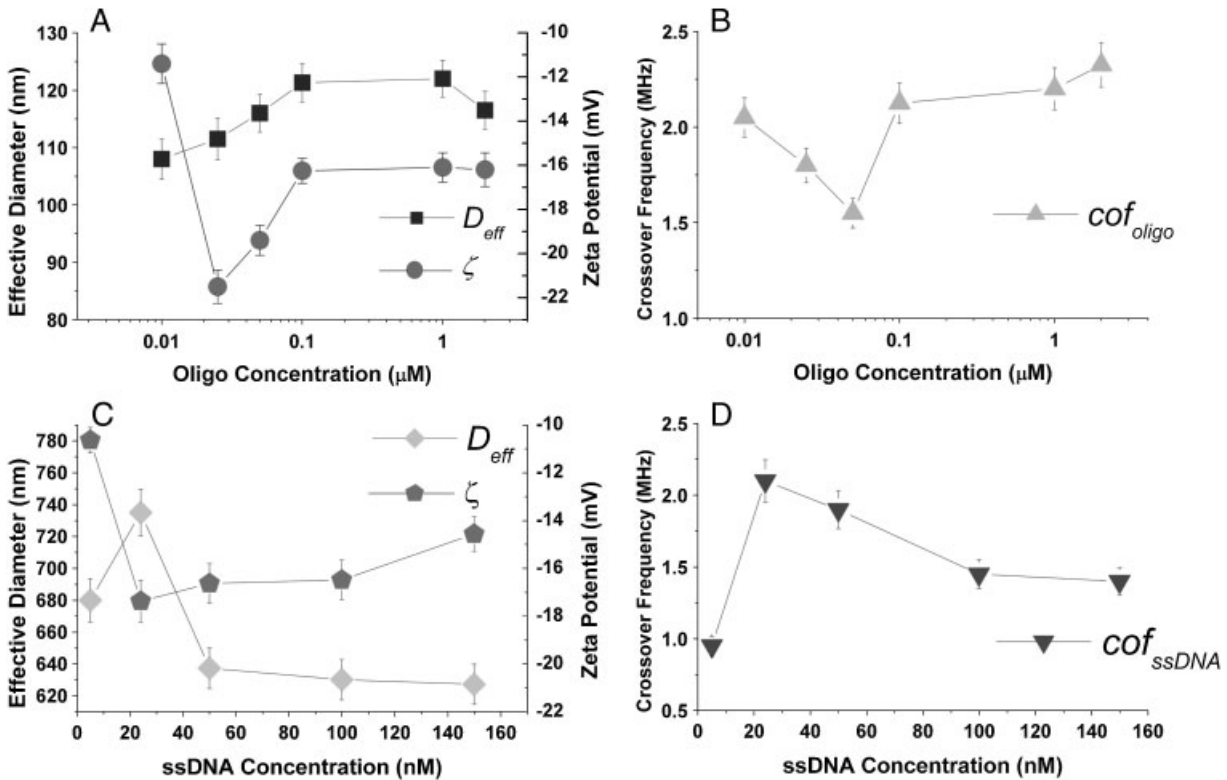
Figure 3. (A) Measured oligonucleotide functionalized particle diameter (■); zeta potential (●). (B) Oligonucleotide functionalized *cof* (▲). (C) Measured ssDNA hybridized particle diameter (⬠); zeta potential (◆). (D) ssDNA hybridized *cof* (▼).

respectively. We present the collective data by normalizing all the parameters with respect to their values at their optimum DNA concentration with the highest particle size, absolute zeta potential and *cof.* As shown in the normalized plot of Fig. 4, the strong correlation among measured particle diameter, zeta potential and DEP *cof* occur for all conditions. This normalized curve offers quantification of the concentration of target ssDNAs above 20 nM. More in-depth tuning of particle size, oligo surface density, oligo/DNA lengths and particle number is under way to reduce this calibration curve to the pM scale.

Based on the observed correlation between particle size, zeta potential and *cof* it is obvious that ssDNA reactions modify the electrical properties of the nanoparticles. With respect to particle size, it is well known that the *cof* should scale as the usual inverse particle relaxation time, $D/\lambda a$, where D, λ and a are the ion diffusion coefficient, double layer thickness and particle diameter, respectively [7]. Physically, as the particle size increases, the time for ions to migrate across the particle surface increases, thus leading to a decrease in the particle *cof*. From this argument, the *cof* is expected to scale inversely with particle size. However, from the data shown in Fig. 3, it appears that this is not the case, as at first glance, particle size appears to scale linearly with *cof*, violating this well-accepted scaling argument. There is hence another mechanism at play in addition to the small, ~12%, change in particle size for each change in DNA surface conformation. A more appropriate explanation of
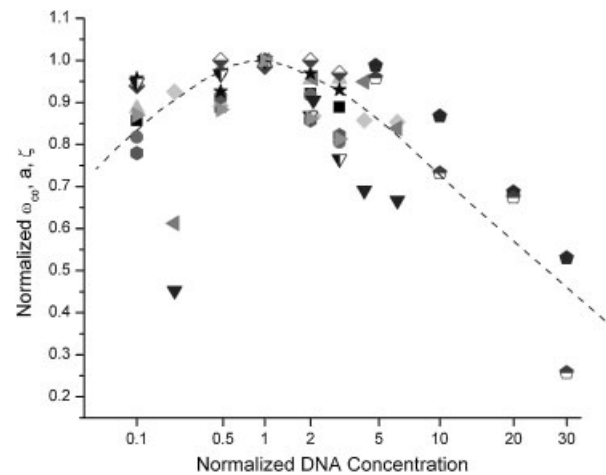

Figure 4. Normalized plots for 100 nm carboxylated nanocolloids functionalized at oligo-ssDNA concentrations of normalized ζ – 0.01 μM (◀), 0.1 μM (▼), 1 μM (▽) and 2 μM (▶); normalized *cof* – 0.01 μM (◆), 0.05 μM (●), 0.1 μM (⬣), 1 μM (▲) and 2 μM (■); normalized particle diameter – 0.01 μM (⬇), 0.1 μM (★), 1 μM (⬤) and 2 μM (⬢).

the observed trend lies in the influence of the particle zeta potential with *cof*. From the data, there appears to be an inverse scaling between zeta potential and particle *cof* for increasing ssDNA concentration, in that as the zeta potential increases or decreases the *cof* is observed to decrease or increase, respectively. Assuming negligible effect on *cof* with

particle size, changes in *cof* can presumably only take place if one increases or decreases the particle conductivity. From the CM factor, one can see that as σ_p increases, the *cof* decreases, while a decrease in σ_p leads to an increase in *cof*.

Completing this argument, one must now look at how changes in particle conductivity relate to changes in zeta potential. The zeta potential is nothing more than the electric potential at the interface between the stern and diffuse layer of the double layer, commonly referred to as the shear plane [14]. As this shear plane increases further away from the particle surface the zeta potential decreases. Depending on the ssDNA surface conformations this shear plane will be located close to the particle surface, for a collapsed or coiled structure, and further away from the surface when the ssDNAs form a more stretched conformation. One can then see from Fig. 3C that the measured zeta potential is at a minimum when the effective particle diameter is greatest, due to the extension of the shear plane with the ssDNA stretched conformation. Finally, the effect of σ_p can now be considered. At the low values of zeta potential the charged ssDNA is bound tightly to the particle surface, leading to an increase in particle surface conductance and a low *cof*. The highest measured *cof* occurs when the particle is least conductive. Presumably this occurs when the ssDNA is not bound tightly to the surface or undergoes a stretched conformation. As expected, this occurs when the shear plane is furthest away from the particle surface, at values of lowest zeta potential.

5   Concluding remarks

In summary we have shown that DEP *cof* can be accurately employed to not only detect whether a carboxylated nano-genetic colloid suspension has undergone functionalization and hybridization but also deduce the conformation of the hybridized DNA. The conformation is concentration-sensitive and the normalized *cof* calibration curve of Fig. 4 offers quantitative estimate of the target ssDNA concentrations.

On the two sides of the DEP *cof*, the nano-genetic colloid suspensions exhibit very different patterns near a micro-fabricated quadrupole electrode, thus allowing feasible hybridization detection *via* label-free digital microscopy. This detection platform is most suited for field applications, as the periphery equipment is available in versions that are small and portable.

The authors have declared no conflict of interest.

6   References

[1] Perraut, F. *et al.*, *Biosens. Bioelectron.* 2008, *23*, 987–994.

[2] Kang, B. S., Pearton, S. J., Chen, J. J., Ren, F. *et al.*, *Appl. Phys. Lett.* 2006, *89*, 122102-(1–3).

[3] Morgan, H., Green, N. G., *AC Electrokinetics: Colloids and Nanoparticles*, Research Studies Press, Herthford-shire, UK 2003.

[4] Pohl, H. A., *Dielectrophoresis*, Cambridge University Press, Cambridge, UK 1978.

[5] Huges, M. P., *Nanoelectromechanics in Engineering and Biology*, CRC Press, Boca Raton, FL 2003.

[6] Cheng, I. F., Chang, H. C., Hou, D., Chang, H.-C., *Biomicrofluidics* 2007, *1*, 021503-(1–15).

[7] Basuray, S., Chang, H.-C., *Phys. Rev. E* 2007, *75*, 060501(R)-(1–4).

[8] Green, N. G., Morgan, H., *J. Phys. Chem. B* 1999, *103*, 41–50.

[9] Verpote, E., *Lab Chip* 2003, *3*, 60N–68N.

[10] Staros, J. V., Wright, R. W., Swingle, D. M., *Anal. Biochem.* 1986, *156*, 220–222.

[11] Milner, S.T., *Science* 1991, *251*, 905–914.

[12] Bloomfield, V.A., *Biopolymers* 1998, *44*, 269–282.

[13] Gelbart, W. M., Bruinsma, R. F., Pincus, P. A., Parsegian, V. A., *Phys. Today* 2000, *23*, 38–44.

[14] Probstein, R. F., *Physicochemical Hydrodynamics*, Wiley, New York 1994.